Estimating the Leaf Area Index of crops through the evaluation of 3D models

Conference Paper · September 2017

DOI: 10.1109/IROS.2017.8206517

4 authors:

Dimitris Zermas
Sentera, INC, Minneapolis MN, United States
13 PUBLICATIONS **64** CITATIONS
SEE PROFILE

Vassilios Morellas
University of Minnesota Twin Cities
81 PUBLICATIONS **1,005** CITATIONS
SEE PROFILE

David J. Mulla
University of Minnesota Twin Cities
236 PUBLICATIONS **5,976** CITATIONS
SEE PROFILE

Nikolaos Papanikolopoulos
University of Minnesota Twin Cities
406 PUBLICATIONS **7,978** CITATIONS
SEE PROFILE

Estimating the Leaf Area Index of Crops Through the Evaluation of 3D Models

Dimitris Zermas[1], Vassilios Morellas[1],
David Mulla[2] and Nikolaos Papanikolopoulos[1]

[1]Department of Computer Science and Engineering, University of Minnesota
[2]Department of Soil, Water and Climate, University of Minnesota

***Abstract*— Financial and social elements of modern societies are closely connected to the cultivation of corn. Due to the massive production of corn, deficiencies during the cultivation process directly translate to major financial losses. The early detection and treatment of crops deficiencies is thus a task of great significance. Towards an automated health condition assessment, this study introduces a scheme for the computation of plant health indices. Based on the 3D reconstruction of small batches of corn plants, an alternative to existing cumbersome Leaf Area Index (LAI) estimation methodologies is presented. The use of 3D models provides an elevated information content, when compared to planar methods, mainly due to the reduced loss attributed to leaf occlusions. High resolution images of corn stalks are collected and used to obtain 3D models of plants of interest. Based on the extracted 3D point clouds, an accurate calculation of the Leaf Area Index (LAI) of the plants is performed. An experimental validation (using artificially made corn plants used as ground truth of the LAI estimation), emulating real world scenarios, supports the efficacy of the proposed methodology. The conclusions of this work, suggest a fully automated scheme for information gathering in modern farms capable of replacing current labor intensive procedures, thus greatly impacting the timely detection of crop deficiencies.**

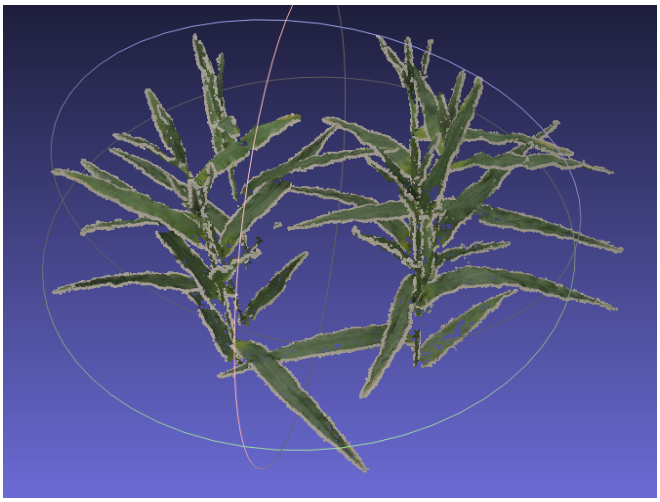

Fig. 1: Example of a 3D model reconstructed by imagery. Six artificial corn stalks are used to automatically extract the biomass without the presence of humans.

I. Introduction

The cultivation of corn crops plays a key role in the financial and social aspects of modern societies. Precision Agriculture (PA) schemes involving aerial and ground surveillance systems, have been developed in an effort to optimize the yield of corn fields; such approaches are mainly concerned with high altitude scanning of the fields by multispectral cameras and manual scanning of a limited number of plants with specialized and expensive sensors. Recent advancements in the area of Computer Vision can pave the way for new and robust solutions targeting PA problems via a thoughtful and in-context transfer of cutting edge vision methodologies.

A review of the existing literature in PA, as presented in Section II, indicates the need for accurate and frequent biomass estimation. For agricultural applications the biomass is a powerful index due to its immediate connection with the crops' health condition and growth state. An accurate model of the corn's canopy can reveal important information regarding the state of corn crops and provide feedback to growth models.

In contrast to existing invasive methods for accurate biomass calculation that rely on plant deconstruction, their non-invasive alternatives are preferred in commercial applications since they leave the crops intact. These state of the art solutions approximate the real LAI with models that measure the light reflectance differences above and below the canopy [1]. The average of several such measurements provides a single result that characterizes a wide area. The spatial sparsity of these methods in combination with the use of cumbersome sensors which are handled by a human impose significant constrains in the sampling process; collecting measurements for a large number of points over the field can be prohibitive, costly and inaccurate. An automated methodology for providing detailed and reliable biomass information from 3D models of corn canopies would directly address the needs of both researchers and companies interested in corn development.

Previous work by Zermas et al. [2] presented a methodology for identifying Nitrogen deficiencies in individual corn plants during the early stages of their development, using RGB images taken from a UAV. Further experimentation suggested that depending on the soil type, such deficiencies may show late, in which case the damage to the plant is irreversible. On the other hand, the LAI information can be used to detect plant stress without such limitations,

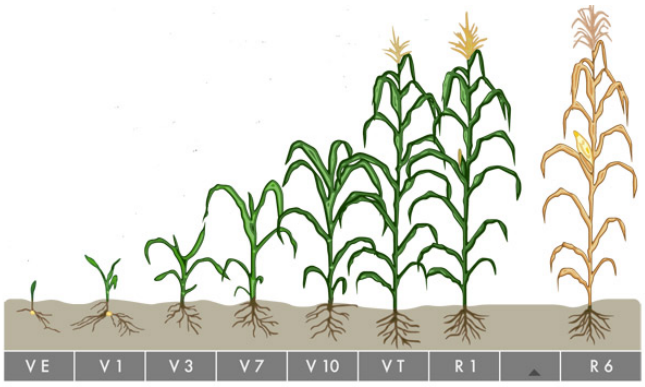

Fig. 2: The growth stages of corn plants are characterized by a letter followed by a number (e.g. "V5"). The letter "V" symbolizes the vegetative stage of the corn, while the number shows how many leaves have grown a visible collar around the stem [3]. Stage VT comes when the last branch of the tassel is completely visible, and the stages characterized by "R" indicate the reproductive stages when the kernel develops and matures.

making it a great candidate for plant pathology assessment. Unfortunately, computing the LAI is nearly impossible with the standard 2D visualization, because occlusions can not be alleviated. To address this drawback, this paper proposes a methodology capable of estimating the LAI of a group of plants using their 3D models. When a 3D model such as in Fig. 1 is accessible, the surface of all of its leaves should be observable, overcoming the leaf occlusions and resulting to a more accurate volumetric information about the plants' biomass.

The proposed methodology is focusing on maize of growth stages between "V5" and "V10" [3], when the plants are still susceptible to treatment and introduces the first attempt for a low-cost, mobile, and easily deployable solution for automated computation of the plant's LAI. For the reader's education, figure 2 demonstrates the different growth stages of corn plants. Initially, high resolution images of the same group of corn plants are collected and a dense 3D model of the canopy is created. The proposed LAI estimation methodology is applied next, yielding information about the health condition of the reconstructed area.

In Section II related work is presented, while Section III describes in more detail the technical aspects of this work, followed by a set of experimental validations summarized in Section IV. In order to assess the accuracy of the proposed LAI estimation procedure, we intentionally experimented with artificial corn plants whose LAI was measured and used as the ground truth. Finally, Section V aggregates the results of this paper and suggests topics for future work.

II. Literature Review

In the agriculture literature a common measure that indicates the biomass of the plant is the LAI. This dimensionless quantity is defined as the one-sided green leaf area per unit ground surface area [4]. This rather vague definition can receive several practical definitions depending on the plant species, the leaf shape and the particular application [5].

For broadleaf plants such as corn, LAI can be computed either directly by destructive sampling of canopy leaves, or indirectly by approximate techniques that involve 2-D imaging and solar radiation measurements above and below the canopy. Chen et al. [6] and Bréda [7] are presenting and comparing a variety of methods of both direct and indirect LAI estimation techniques. Direct methodologies produce accurate results but are time consuming and destroy the plants. On the other hand, estimating the LAI based on the existing indirect methodologies requires human presence for the collection of data [8], and may result in estimation errors of up to 25% because of occlusions and cluttering introduced by the dense canopies [9].

Although the need for a detailed 3D model of the corn canopy was apparent even in the early stages of PA ([10] and [11]), the 3D reconstruction applications in PA are limited and targeted mainly towards the estimation of plant biometrics. Most relative is the work of Wang et al. [12] who are presenting a 3D reconstruction technique for a single corn plant based on the shape of the leaves' outline while making several assumptions in order to acquire a very accurate 3D model. Dong et al.[13] and Carlone et al. [14] propose a model for the estimation of the plant's height over time. Recently, Qu et al.[15] presented a real time 3D reconstruction sensor for various agricultural applications, and Kjaer et al. [16] have been experimenting with 3D reconstruction from near-infrared 3D scanners in order to assess the nutrient state of plants in controlled environments.

Although targeting barley instead of corn, the importance of biomass in plant growth is being stressed by the work of Aasen et al. [17], Bendig et al. [18], and Tilly et al. [19]. The most notable difference of these publications versus the current work is the scale in which the problem is approached. Their solution creates 3D models of a large part of the farm, while ours targets a small group of plants providing more detailed information of individual plants and leaves.This detailed and small scale 3D plant reconstruction is important as we deploy this model to measure the leaf area with a method discussed in the upcoming sections.

Other notable publications regarding 3D reconstruction and measurement of plants include Biskup et al. [20], that use stereo vision to get geometric characteristics of the canopy, and Klose et al. [21], who discuss the usability of Time-of-Flight (ToF) cameras in PA. Lastly, Alenya et al. [22] also utilize ToF sensors as a complement to RGB cameras to gain access to broader range of measurements. In these last three cases it is noted that experiments are conducted in completely controlled indoor environments.

III. Methodology

The core methodology for the computation of LAI as presented in this section requires a dense 3D reconstruction of a group of plants. This can be obtained by capturing high resolution images of the targeted group while moving in a circular fashion as seen in Fig. 3 and employing a 3D reconstruction toolbox such as [23]. Obtaining the 3D model decoupled from the point cloud processing does not

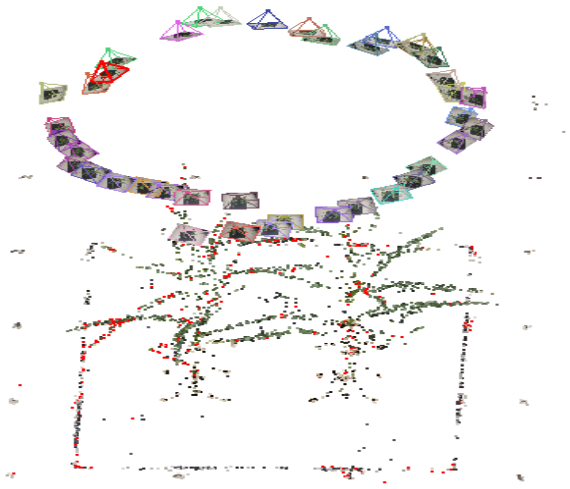

Fig. 3: The sparse reconstruction resulting from the VisualSFM software. In this non-limiting example, several high resolution images were taken using a handheld camera while moving in a circular fashion around six artificial corn stalks.

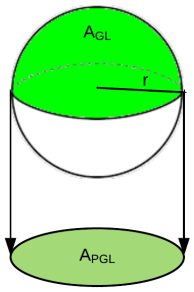

Fig. 4: A simple example to explain the definition of LAI. The total area of the green part of the sphere symbolizes the area of the green leaves and is $2\pi r^2$ (r is the radius), while the orthogonally projected area is a circle of area πr^2. Therefore, LAI = $2\pi r^2/\pi r^2 = 2$.

impose any platform constraints and only requires an RGB sensor and sufficient computation capabilities. It is possible to acquire the necessary imagery through handheld or UAV mounted cameras.

A. Interpreting the 3D Reconstruction

Once the 3D model is obtained, an assessment on the condition of the canopy is made. Initially, the soil plane is detected and removed using RANdom SAmple Consensus (RANSAC) [24] to estimate the coefficients of the ground plane. This results in a point cloud $P \in \mathbb{R}^3$ that consists only of points belonging to the plants which is then used to provide volumetric information.

A popular interpretation of the LAI when dealing with canopy imaging considers the ratio of the total area of the green leaves to the area of the green leaves when they are projected on the ground:

$$LAI = A_{GL}/A_{PGL}, \quad (1)$$

with A_{GL} denoting the **A**rea of the **G**reen **L**eaves and A_{PGL} the **A**rea of the **P**rojected **G**reen **L**eaves. This interpretation of the LAI index receives values ≥ 1 since A_{PGL} is generally smaller than A_{GL} considering the various occlusions amongst leaves [25].

In order to estimate the LAI based on its original definition as provided by Eq. 1, we need to compute the two quantities that correspond to i) the one-sided green leaf area (A_{GL}) and ii) the unit ground surface area (A_{PGL}).

B. Leaf Segmentation

At first, the computation of A_{GL} requires the segmentation of each one of the leaves of the depicted plants. For the growth stage of the plants we are interested in ("V5" to "V10"), the canopy is not particularly dense and most of the individual leaves are observable during the 3D reconstruction.

Still, occlusions and leaf intersections are present leading to a non-trivial segmentation process which concludes in two steps. Initially, a clustering technique such as the euclidean cluster extraction combined with a statistical outlier removal [26] is employed to break down the point cloud P into N clusters of 3D points $P_i \subset P$ with $i = 1, \ldots, N$, each containing one or more single leaves, with examples seen in Fig. 5.

The second step of the segmentation needs to iterate over all N clusters, leave the single leaf clusters intact, and break apart the clusters that contain more than one leaf. For this purpose a 3D skeletonization technique is employed [27] which acts on each point cluster P_i and delivers a skeleton S_i comprised from a set of connected nodes $s \subset S_i$. Each node is the centroid of a collection of neighboring 3D points and acts as their representative.

The nodes capture the topology of the leaves, which is used by our proposed algorithm to achieve a refined segmentation. In particular, we assume only three types of nodes s; namely the endpoint nodes, the intersection nodes, and the standard nodes. Endpoints are nodes with only one immediate neighbor, while intersections have more than two immediate neighbors and standard points have exactly two.

Under this definition, we assume that any endpoint node signifies one end of a single leaf and that starting from an endpoint, a set of neighboring standard and intersection nodes in a smooth trajectory forms the midrib of the leaf. Referring to Fig. 6, one can see the nodes $s_1, \ldots, s_{10}$ and $s_{11}, \ldots, s_{17}$ forming the two leaf midribs while both curves start from an endpoint. Although we assume the midribs to start from an endpoint, it is possible for them to end at any node and the decision is based on the smoothness of the curve.

In order to define a criterion for the smoothness of a curve, we treat the nodes of a the skeleton as measurements of the trajectory of a physical object in 3D and employ a Kalman filter to decide whether a node belongs to the midrib or

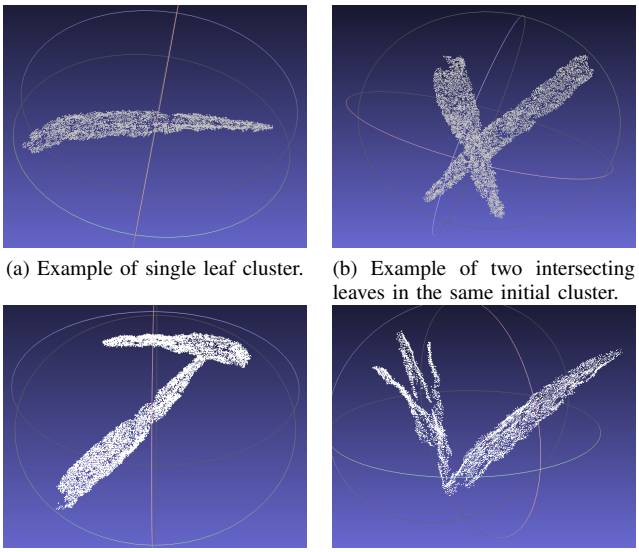

(a) Example of single leaf cluster.

(b) Example of two intersecting leaves in the same initial cluster.

(c) Example of two touching leaves in the same initial cluster.

(d) Example of four leaves at the top of a single plant in the same initial cluster.

Fig. 5: Example of clusters produced by the initial euclidean clustering step. Cases like (a) do not need extra refinement since the initial cluster represents a single leaf. In the contrary, cases like (b), (c), and (d) need to be further refined to produce single leaf clusters.

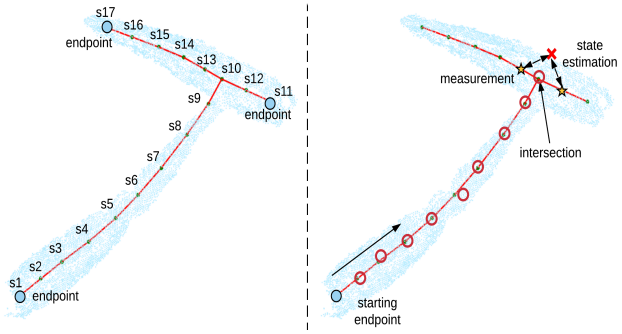

Fig. 6: *Left:* Example of a 3D skeleton of two overlapping leaves. Three endpoint nodes (s_1, s_{11}, and s_{17}), one intersection node (s_{10}), and several standard nodes ($s_2 - s_9$, s_{12}, and $s_{13} - s_{16}$) are visible. *Right:* Example of the SKF algorithm starting from node s_1. Kalman filtering is used iteratively to make decisions on the nodes that belong to the midrib. The red circles represent estimates on the position of the nodes x_{kest} that have been found to be close to their respective node-measurements (green dots). The red cross presents the position estimate that is far away from its respective measurements (yellow stars), thus signifying that s_{10} is an end-node for the particular leaf.

not. This segmentation refinement process we call Skeleton Kalman Filtering (SKF). Specifically, we employ the model:

$$x_k = x_{k-1} + v_{k-1}\Delta t + \frac{1}{2}\alpha\Delta t^2 \qquad (2)$$
$$v_k = v_{k-1} + \alpha\Delta t$$

which is transformed, as used in Kalman filtering, in the matrix form:

$$\begin{pmatrix} x_k \\ v_k \end{pmatrix} = \begin{pmatrix} I_3 & I_3\Delta t \\ 0_3 & I_3 \end{pmatrix} x_{k-1} + \begin{pmatrix} \frac{\Delta t^2}{2} \\ \Delta t \end{pmatrix} \alpha \qquad (3)$$

with $x_k = [x, y, z]^T$, $v_k = [\dot{x}, \dot{y}, \dot{z}]^T$, $\Delta t = 1$, $\alpha = 0.01$, $I_3 \in R^{3x3}$ identity matrix, and $0_3 \in R^{3x3}$ zero matrix. At the same time, the measurements $z_k = [z_{kx}, z_{ky}, z_{kz}]^T$ take the form:

$$z_k = \begin{pmatrix} I_3 | 0_3 \end{pmatrix} x_{k-1}, \qquad (4)$$

and the model and measurement uncertainty matrices Q and R respectively are:

$$Q = \begin{pmatrix} I_3\frac{\Delta t^4}{4} & I_3\frac{\Delta t^3}{2} \\ I_3\frac{\Delta t^3}{2} & I_3\Delta t^2 \end{pmatrix}, \; R = \begin{pmatrix} I_3\sigma^2 \end{pmatrix}, \qquad (5)$$

with $\sigma = 0.1$.

The position part x_k of the state vector is initialized with the first endpoint of the midrib, velocity $v_k = [0, 0, 0]^T$ and the Kalman filter is applied iteratively. At each iteration the estimated position x_{kest} is compared with the next neighboring node(s) (that act as measurements z_k) and based on a distance threshold the node is considered part or the end of the midrib.

$$||x_{kest} - z_k||_2 < d_{threshold}. \qquad (6)$$

As seen in the right image of Fig. 6, the skeleton branch that initiates from the starting endpoint s_1 applies Kalman filtering and adds the standard points up to s_{10} to the midrib. The filter estimates that the next node s_{11} should be at the red cross for the smoothness of the midrib to persist. Nevertheless, the actual neighboring nodes (yellow stars) are not consistent with the estimate meaning that the intersection node s_{10} signifies the end of the leaf.

C. Leaf Area Computation

Even with the refinement step of SKF, significant problems manifest with the creation of a 3D point cloud due to noisy measurements and textureless leaf areas. In particular, noise corrupted points that were originally part of the actual leaf surface are reconstructed away from it and are hard to detect and correct. Furthermore, lack of texture generates large uneven holes in the central parts of the leaves that require supervised hole filling algorithms [28] in order to create a meaningful surface for the area computation.

A computationally efficient algorithm that produces satisfactory results overcoming the aforementioned limitations is the Self-Organized Map (SOM) [29]. Utilizing two fully connected layers of a neural network, SOM is an unsupervised algorithm which creates a grid that organizes itself to capture the topology of the provided data. The SOM is undertaking an automatic smoothing of data by fitting this grid of points according to the density of the recorded data, thus minimizing fitting error in densely reconstructed areas. The grid, also known as lattice, provides flexibility in that its granularity is controlled at will by the user. Altering this

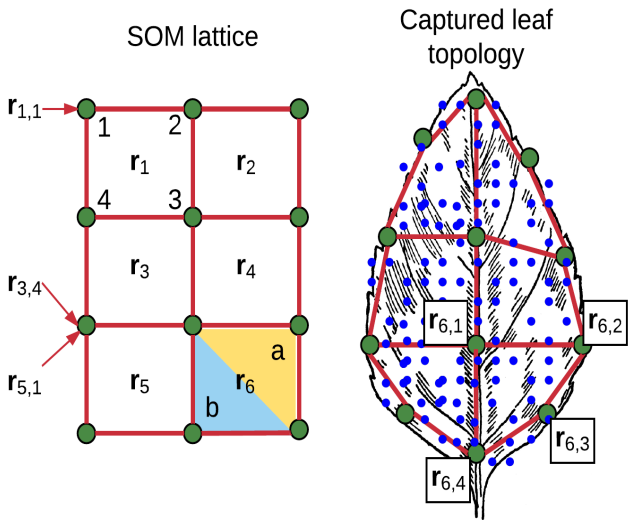

Fig. 7: The Self-Organized-Map (SOM) lattice (left) is adapting to the surface of the leaf (right) capturing the topology of the reconstructed points. *Left:* Each square in the lattice receives an identification label r_u and its four vertices (larger dots) are numbered in a clockwise fashion starting from the top left $v = 1, 2, 3$, or 4. This way, the computation of the area through the two triangles (a and b) is feasible. *Right:* The lattice assumes the reconstructed points' (small dots) topology. On a 3D surface, the SOM lattice resembles a membrane that stretches around the 3D points. An example of the sixth polygon's indeces is visible inside the squares.

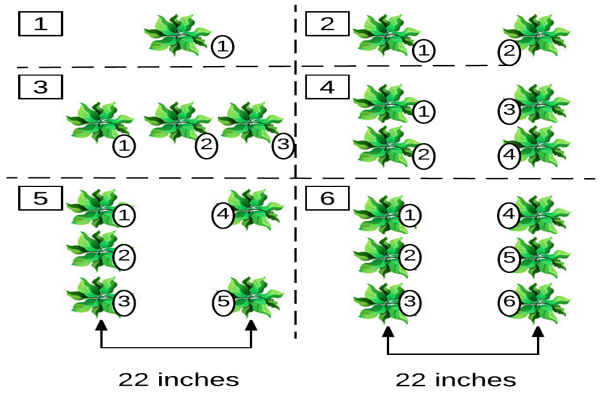

Fig. 8: The experimental setup involved six different corn plant configurations with increasing complexity. The numbers inside the squares depict the experiment number and the numbers in the circles represent the plant identification. One to six plants were used in realistic scenarios keeping distances between rows at 22 inches, a standard corn row distance used at the United States farmlands.

parameter can achieve higher execution speed so that the estimation of the LAI is performed without affecting the accuracy to undesirable levels.

In our case, the provided data is a point cloud of a leaf and the SOM is used to express the surface of the leaf so that the area computation is feasible. When the SOM converges to its final form (Figure 9c), several four-edged polygons with known vertices cover the surface of the leaf and are identified as $r_{u,v}$, with $u = 1, \ldots, K$ number of polygons and $v = 1, 2, 3$, or 4 the number of the vertex in a clockwise order (Fig. 7). Each polygon is then broken down into two triangles by indexing its four vertices v in order $1 \rightarrow 2 \rightarrow 3$ (triangle a) and $3 \rightarrow 4 \rightarrow 1$ (triangle b). The total area of the surface can be approximated by adding the areas of all the triangles. Finally, the total green leaves area (A_{GL}) is the summation of the areas of the individual leaf clusters.

A_{PGL} can be computed in a simpler manner. First, all the vertices of the SOM lattice are treated as 3D points and are projected on the ground with the projection matrix:

$$T = I_3 - nn^T \in \mathbb{R}^{3x3}, \tag{7}$$

with $I_3 \in \mathbb{R}^{3x3}$ the identity matrix and $n \in \mathbb{R}^3$ the normal vector of the ground plane. The projected points form a concave two dimensional polygon in 3D which is used to create a mesh of triangles that occupy the desired area. An occupancy grid with known cell size is generated and overlayed ontop of the mesh to determine how many cells are occupied. Again, adding the area of all the occupied cells provides an estimation of A_{PGL}.

The 3D reconstruction resulting from an SfM algorithm is up-to-scale equivalent to the actual scene, which means that the computed A_{GL} is not directly comparable to the groundtruth measurements. Our solution in determining the scaling factor s of the reconstruction in order to verify the correctness of our computations is to compare the height of the artificial corn plants h_{real} against the height of the reconstructed corn plants $h_{reconstructed}$, and use their ratio as the scaling factor for the whole point cloud:

$$s = \frac{h_{real}}{h_{reconstructed}}. \tag{8}$$

IV. Experimental Results

The experimental results section illustrates the sequence of steps for the computation of the leaf area index on the produced point cloud.

A. Experimental Setup

The reproducibility of the experiments and the accuracy in the collection of the ground truth measurements contributed to our decision to validate our LAI estimation algorithm on artificial corn stalks that are based on real corn models at a "V6" growth stage (the number of developed collars on the stem is 6).

A total number of six artificial plants with similar biometrics were used and the areas of their leaves was approximated by the formula: $L * W * k$, with L the length of the leaf from the stem to the tip, W the maximum width, and the constant $k = 0.75$ was selected based on literature as a viable approximation of the leaf area [30].

The 3D reconstructions were created offline using the VisualSFM toolbox [23] with the number of input images varying from 18 to 24 and the images were collected with a handheld Olympus TG-4 camera of 1440x1920 pixel resolution. A sample sparse reconstruction output from the VisualSFM toolbox can be seen in Fig. 3, while dense reconstruction results of real and artificial corn produced via

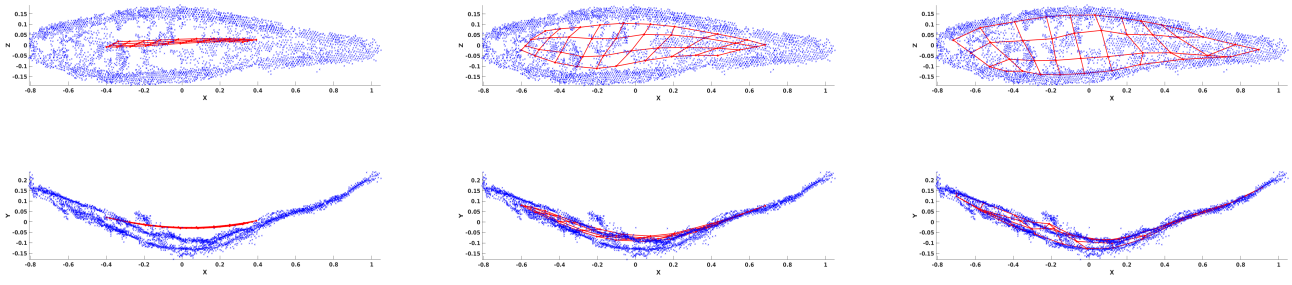

(a) $t = 200$ (b) $t = 1000$ (c) $t = 6000$

Fig. 9: Progression of the Self-Organized Map. The initial lattice (red grid) is iteratively trying to capture the topology of the leaf (blue dots represent the 3D points of the leaf). The outliers are ignored and the resulting surface is resembling the real leaf despite the reconstruction errors. Top row is a top-down view of the leaf, bottom row is a lateral view. t symbolizes the time step in the algorithmic process. In MatLab the average processing time of one leaf is 0.52 seconds.

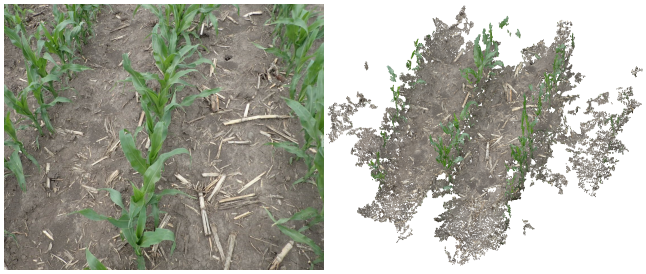

Fig. 10: *Left:* One of the images use for the construction of the 3D model visible on the right. *Right:* The dense 3D reconstruction of real corn plants in the field is provided as reference for visual comparison with the artificial corn.

the use of the PMVS tool [31] are seen in the Figures 1, 10 and 12b.

B. Interpreting the 3D Reconstruction

We are considering six different configurations of artificial corn stalks with increasing complexity which, as seen in Fig. 8, try to mimic realistic scenarios and assist in verifying the sensibility of the proposed method. In experiment #1 a single plant is reconstructed showing how the algorithm behaves with minimal occlusion. The same goes for experiment #2 where non-overlapping leaves are considered in a standard 22 inch distance between two corn rows. Experiments #3 through #6 show cases of severe overlap and occlusion with increasing number of plants and #5 shows a case where the row is missing a plant due to seeding error. The results of the preprocessing methodology described in section III-A are depicted step by step for the most complex scenario (experiment #6) in Fig. 12. A lateral view of the six corn stalks can be seen in 12(a), while the 3D reconstruction is visible in 12(b). In 12(c), the leaves have been segmented using the SKF methodology. Lastly, 12(d) shows the projection of the two corn stalks of the ground.

Results on the algorithm that estimates the area of the leaves is present in Figure 9. The figure shows the expansion of the network over several iterations until it converges. Two viewpoints are provided to clarify the progress steps. The SOM algorithm has proven to be particularly robust and manages to adapt to the data providing a leaf-like shape and overcoming limitations such as noise 13(a), small number of points 13(b) and sparse reconstruction 13(c).

		No. of Experiment					
		1	2	3	4	5	6
Corn Stalk ID	a	0.1198	0.1062	0.1205	0.1392	0.1328	0.1216
	b	-	0.1241	0.1137	0.1361	0.1294	0.1090
	c	-	-	0.1251	0.1103	0.1405	0.1377
	d	-	-	-	0.0989	0.1002	0.1150
	e	-	-	-	-	0.0975	0.1281
	f	-	-	-	-	-	0.1000
	T	0.1198	0.2303	0.3593	0.4845	0.6004	0.7114
	GT	0.1119	0.2238	0.3357	0.4476	0.5595	0.6714
	error	6.59%	2.82%	6.57%	7.62%	6.81%	5.62%
	LAI	1.6954	1.6667	2.6882	2.6994	1.8296	2.7205

TABLE I: Leaf area estimation for each one of the plants in all six experimental setups. The mean ground truth total leaf area for a single artificial plant is $A_{GL} = 0.1119$. Since all six artificial plants are industrially manufactured, we assume they share approximately the same total leaf area. The variable T represents the estimated total leaf area, which is a column-wise sum of each experiment and GT is the groundtruth total area of the reconstructed plants. The LAI is computed for each experiment and presented in the last row.

The validity of the algorithm is assessed by comparing the computed A_{GL} scaled using Eq. 8, against the groundtruthed total leaf area (A_{GL}) measurements. In Table I, each column represents one of the six experiments and the rows hold the estimated leaf area information for each plant. The total leaf area is the sum of the individual plants' leaf area and the accuracy of the methodology is validated by the relative error which is computed as:

$$error = \frac{abs(T - GT)}{GT}. \tag{9}$$

The estimated LAI is presented last for completeness despite the lack of means to compute the groundtruthed projected leaf area (A_{PGL}).

Further, in Fig. 11 we present some examples of single leaf area estimation taken from the most complex experiment #6. An image of the leaf is placed next to its 3D

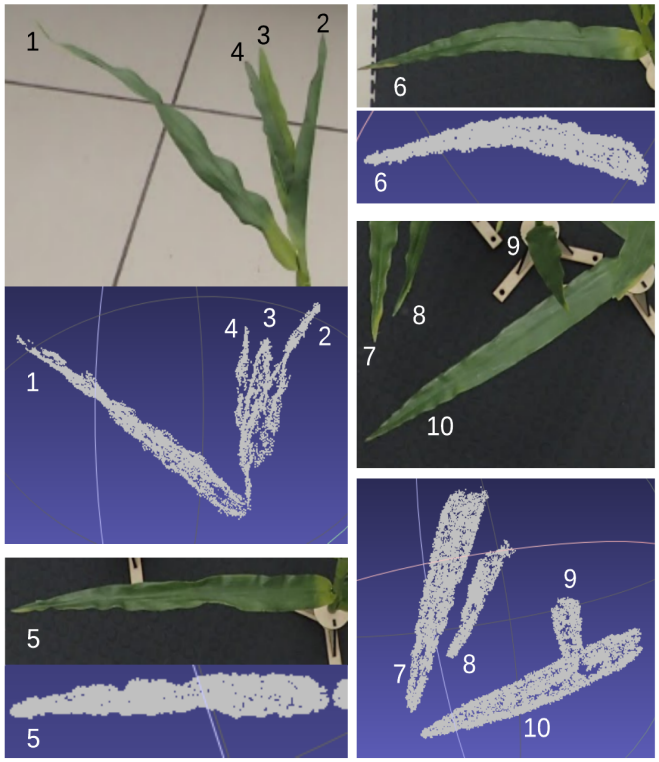

Fig. 11: Several examples of initial images along with their reconstructed pairs are presented. In Table II We provide the estimated area for each leaf along with its groundtruth (GT) value.

Leaf #	1	2	3	4	5
Area	0.0204	0.0062	0.0122	0.0031	0.0320
GT	0.0168	0.0055	0.0051	0.0086	0.0261
Leaf #	6	7	8	9	10
Area	0.0228	0.0210	0.0190	0.0189	0.0295
GT	0.0247	0.0247	0.0165	0.0165	0.0261

TABLE II: This table accumulates the area estimation and groundtruth (GT) of the leaf instances seen in Fig. 11. An interesting observation regarding the leaves #3 and #4 can be made regarding the accuracy of the area estimation. These leaves are too close for the 3D skeletonization algorithm to separate them correctly resulting to one of the two leaves dominating over the other. The summation of their respective estimated areas closely follows the groundtruth.

reconstruction followed by the estimated and groundtruthed values of its area presented in Table II. These results support our proposed methodology and suggest that we may aim for a generalizable version that can be utilized as a tool for the estimation of LAI and the replacement of outdated and labor intensive solutions.

C. Limitations

The proposed methodology depends heavily on the quality of the 3D reconstruction for the segmentation of individual leaves. In the experiments #5 and #6 the density of the canopy occludes the lower leaves resulting in the partial reconstruction of one leaf in both cases. This result does not significantly affect the total area and LAI estimation but indicates some of the limitations of the pipeline.

A partial 3D reconstruction affects the SKF segmentation step which utilizes the 3D skeletonization to separate the independent leaves. When the leaf surface has a large hole

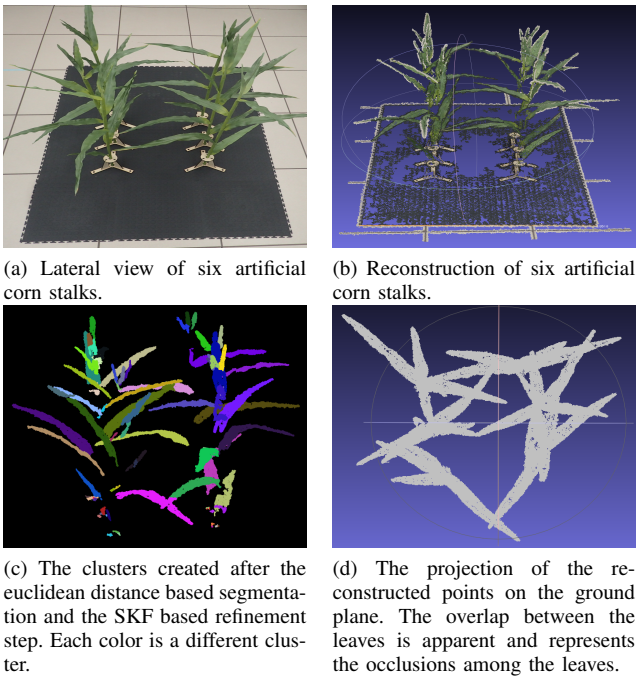

(a) Lateral view of six artificial corn stalks.

(b) Reconstruction of six artificial corn stalks.

(c) The clusters created after the euclidean distance based segmentation and the SKF based refinement step. Each color is a different cluster.

(d) The projection of the reconstructed points on the ground plane. The overlap between the leaves is apparent and represents the occlusions among the leaves.

Fig. 12: Steps for the point cloud preprocessing. Several images similar to (a) create a 3D point cloud (b). The segmented leaves (c) as well as the projection (d) are used to compute the nominator (A_{GL}) and denominator (A_{PGL}) of the LAI.

due to lack of texture in the reconstruction process, the skeleton is forced to create unnecessary branches which may end up in the over-segmentation of the leaf. This problem is partially addressed by the flexibility of the SOM but introduces inaccuracies to the final area computation.

V. Conclusions and Future Work

In this work, we have shown the efficacy of our proposed methodology for the estimation of the LAI of corn plants when their detailed 3D models are provided. Our experiments have shown the feasibility to acquire good enough 3D reconstruction results in a real world and laboratory environment, and have validated the proposed methodology on artificial specimens with known biometrics (Table I and II). Those findings support the importance and applicability of such techniques to real world PA challenges. The obtained results act as a proof of concept for the introduction of a new interpretation to a classic biomass index definition, and show the automation capabilities that field monitoring can achieve through the use of state of the art Computer Vision techniques.

Future work requires the validation of the LAI estimation algorithm over a dataset with real plants in an outdoor environment for the verification of its consistency. Finally, since the operation of the LAI estimation methodology has been established, the introduction of a pipeline for the groundtruthing and 3D reconstruction of real corn plants will be beneficial towards the creation of an open access dataset.

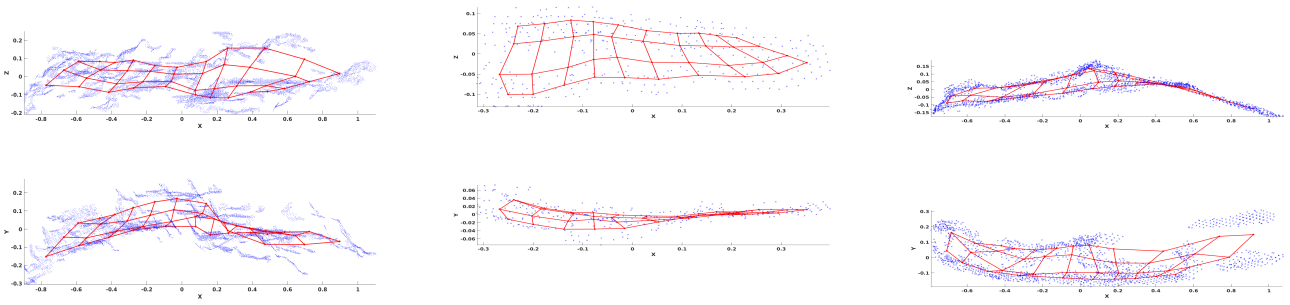

(a) (b) (c)

Fig. 13: Extreme cases of reconstructed leaves validate that the algorithm performs satisfactorily. In (a), a small number of images was used for the reconstruction, resulting in a noisy point cloud. The reconstructed leaf in (b) is small and further away from the camera, therefore its 3D points are fewer and sparse. A significant part of the leaf has not been reconstructed in (c).

ACKNOWLEDGEMENTS

Dimitris Zermas has been supported in part by a UMII Fellowship. This material is based upon work supported by the Corn Growers Association of MN and the National Science Foundation through grants #IIP-0934413, #IIS-1017344, #CNS-1061489, #IIS-1427014, #IIP-1432957, and #CNS-1531330.

REFERENCES

[1] I. Jonckheere, S. Fleck, K. Nackaerts, B. Muys, P. Coppin, M. Weiss, and F. Baret, "Review of methods for in situ leaf area index determination: Part I. Theories, sensors and hemispherical photography," *Agricultural and Forest Meteorology*, vol. 121, no. 12, pp. 19 – 35, 2004.

[2] D. Zermas, D. Teng, P. Stanitsas, M. Bazakos, V. Morellas, D. Mulla, and N. Papanikolopoulos, "Automation solutions for the evaluation of plant health in corn fields," *IEEE Intelligent Robots and Systems (IROS), Hamburg*, 2015.

[3] J. J. Hanway *et al.*, "How a corn plant develops." *How a corn plant develops*, 1966.

[4] D. Watson, "Comparative physiological studies on the growth of field crops: I. variation in net assimilation rate and leaf area between species and varieties and within and between years," *Annals of Botany*, vol. 11, pp. 41–76, 1947.

[5] I. Jonckheere, S. Fleck, K. Nackaerts, B. Muys, P. Coppin, M. Weiss, and F. Baret, "Methods for leaf area index determination. Part I: Theories, techniques and instruments."

[6] J. M. Chen, P. S. Plummer, M. Rich, S. T. Gower, and J. M. Norman, "Leaf area index measurements," *Journal of geophysical research*, vol. 102, no. D24, pp. 29–429, 1997.

[7] N. J. Bréda, "Ground-based measurements of leaf area index: a review of methods, instruments and current controversies," *Journal of experimental botany*, vol. 54, no. 392, pp. 2403–2417, 2003.

[8] W. Wilhelm, K. Ruwe, and M. R. Schlemmer, "Comparison of three leaf area index meters in a corn canopy," *Crop Science*, vol. 40, no. 4, pp. 1179–1183, 2000.

[9] R. Hu, G. Yan, X. Mu, and J. Luo, "Indirect measurement of leaf area index on the basis of path length distribution," *Remote Sensing of Environment*, vol. 155, pp. 239 – 247, 2014.

[10] C. Fournier and B. Andrieu, "A 3d architectural and process-based model of maize development," *Annals of Botany*, vol. 81, no. 2, pp. 233–250, 1998.

[11] H. Sinoquet, S. Thanisawanyangkura, H. Mabrouk, and P. Kasemsap, "Characterization of the light environment in canopies using 3d digitising and image processing," *Annals of Botany*, vol. 82, no. 2, pp. 203–212, 1998.

[12] H. Wang, W. Zhang, G. Zhou, G. Yan, and N. Clinton, "Image-based 3d corn reconstruction for retrieval of geometrical structural parameters," *International Journal of Remote Sensing*, vol. 30, no. 20, pp. 5505–5513, 2009.

[13] J. Dong, L. Carlone, G. C. Rains, T. Coolong, and F. Dellaert, "4d mapping of fields using autonomous ground and aerial vehicles," *ASABE and CSBE/SCGAB Annual International Meeting*, 2014.

[14] L. Carlone, J. Dong, S. Fenu, G. C. Rains, and F. Dellaert, "Towards 4d crop analysis in precision agriculture: Estimating plant height and crown radius over time via expectation-maximization," *Workshop on Robotics in Agriculture, IEEE International Conference on Robotics and Automation (ICRA)*, 2015.

[15] J. Das, G. Cross, C. Qu, A. Makineni, P. Tokekar, Y. Mulgaonkar, and V. Kumar, "Devices, systems, and methods for automated monitoring enabling precision agriculture," *IEEE International Conference on Automation Science and Engineering (CASE)*, pp. 462–469, 2015.

[16] K. Kjaer and C.-O. Ottosen, "3d laser triangulation for plant phenotyping in challenging environments," *Sensors*, vol. 15, no. 6, p. 1353313547, Jun 2015.

[17] H. Aasen, A. Burkart, A. Bolten, and G. Bareth, "Generating 3d hyperspectral information with lightweight UAV snapshot cameras for vegetation monitoring: From camera calibration to quality assurance," *ISPRS Journal of Photogrammetry and Remote Sensing*, vol. 108, pp. 245 – 259, 2015.

[18] J. Bendig, K. Yu, H. Aasen, A. Bolten, S. Bennertz, J. Broscheit, M. L. Gnyp, and G. Bareth, "Combining UAV-based plant height from crop surface models, visible, and near infrared vegetation indices for biomass monitoring in barley," *International Journal of Applied Earth Observation and Geoinformation*, vol. 39, pp. 79 – 87, 2015.

[19] N. Tilly, H. Aasen, and G. Bareth, "Fusion of plant height and vegetation indices for the estimation of barley biomass," *Remote Sensing*, vol. 7(9), 2015.

[20] B. Biskup, H. Scharr, U. Schurr, and U. Rascher, "A stereo imaging system for measuring structural parameters of plant canopies," *Plant Cell Environment*, vol. 30, p. 12991308, Jun 2007.

[21] R. Klose, J. Penlington, and A. Ruckelshausen, "Usability study of 3d time-of-flight cameras for automatic plant phenotyping," *Image Analysis for Agricultural Products and Processes*, p. 93105, 2009.

[22] G. Alenya, B. Dellen, and C. Torras, "3d modelling of leaves from color and tof data for robotized plant measuring," in *IEEE International Conference on Robotics and Automation (ICRA)*, May 2011, pp. 3408–3414.

[23] C. Wu *et al.*, "VisualSFM: A visual structure from motion system," 2011.

[24] M. Y. Yang and W. Förstner, "Plane detection in point cloud data," in *Proceedings of the 2nd int conf on machine control guidance, Bonn*, vol. 1, 2010, pp. 95–104.

[25] W. Wilhelm, K. Ruwe, and M. R. Schlemmer, "Comparison of three leaf area index meters in a corn canopy," *Crop Science*, vol. 40, no. 4, pp. 1179–1183, 2000.

[26] R. B. Rusu, "Semantic 3d object maps for everyday manipulation in human living environments," Ph.D. dissertation, Computer Science department, Technische Universitaet Muenchen, Germany, October 2009.

[27] J. Cao, A. Tagliasacchi, M. Olson, H. Zhang, and Z. Su, "Point cloud skeletons via Laplacian based contraction," in *Shape Modeling International Conference (SMI), 2010*. IEEE, 2010, pp. 187–197.

[28] M. Kazhdan, M. Bolitho, and H. Hoppe, "Poisson surface reconstruction," in *Proceedings of the fourth Eurographics symposium on Geometry processing*, vol. 7, 2006.

[29] T. Kohonen, "Self-organizing maps," *Series in Information Sciences*, vol. 30, 1997.

[30] E. G. Montgomery, "Correlation studies in corn," in *24th Annual Report, Nebraska, Mo, USA*. Agricultural Experiment Station, 1911.

[31] Y. Furukawa and J. Ponce, "Accurate, dense, and robust multiview stereopsis," *IEEE Transactions on Pattern Analysis and Machine Intelligence*, vol. 32, no. 8, pp. 1362–1376, Aug 2010.